

Ab initio study of transition paths between (meta)stable phases of Nb and Ta-substituted Nb

Susanne Kunzmann,^{1,2,3} Thomas Hammerschmidt,³ Gabi Schierning,^{1,2,4} and Anna Grünebohm^{3,5}

¹*Experimental Physics, Bielefeld University, Universitätsstr 25, 33615 Bielefeld, Germany*

²*Research Center Future Energy Materials and Systems (RC FEMS),
University of Duisburg-Essen, Forsthausweg 2, 47057 Duisburg, Germany*

³*Interdisciplinary Centre for Advanced Materials Simulation (ICAMS),
Ruhr-University Bochum, Universitätsstr 150, 44801 Bochum, Germany*

⁴*Center for Nanointegration Duisburg-Essen (CENIDE),
University of Duisburg-Essen, Forsthausweg 2, 47057 Duisburg, Germany*

⁵*Center for Interface-Dominated High Performance Materials (ZGH),
Ruhr-University Bochum, Universitätsstr 150, 44801 Bochum, Germany*

(Dated: October 30, 2023)

Although Niobium is a well characterized material it still shows some anomalies that are not yet understood. Therefore we revisit its metastable phases using density functional theory. First, we systematically compare energies and ground state volumes of chosen crystal structures and discuss possible transition paths to the bcc ground state structure and the energy landscape for tetragonal distortions. Furthermore, we discuss their stability by means of their phonon spectra and vibronic free energies. Second we analyze the impact of tantalum impurities on phase stability. Surprisingly we find new aspects of the energy landscape of the material which have been overlooked so far: A new local energy minimum on the bcc to omega transition path, a flat energy landscape with respect to uniaxial strain along [111] and a considerable stabilization of the σ phase by Ta substitution.

I. INTRODUCTION

Niobium (Nb) is one of the best studied elemental metals. Nevertheless, and surprisingly, several properties of this material remain unexplained. For instance, it has the highest superconducting transition temperature of all elements at normal pressure,¹ but there is still debate about the character of its superconductivity.^{2,3} Nb is one of the few transition metals that exist in a bcc ground state. However, depending on the boundary conditions, there are many different metastable phases, especially under high pressure^{4,5} or in nanostructures,^{6,7} but their relative stability and potential transition pathways are not yet fully understood. Remarkably, Bollinger et al.⁸ experimentally found a change of the slope in the linear thermal expansion coefficients of the bcc state by high-resolution calorimetry at 208 K and related this to a potential martensitic phase transition. However, the signatures of this phase transition were smaller than the detection limit of x-ray diffraction, and hence the nature of this phase transition remained poorly understood.

Martensitic phase transitions are only possible if there is a diffusionless transition path with a moderate energy barrier connecting both the ground state structure and the metastable phase. Especially in metals, such phase transitions with their complex interplay of phononic, electronic and microstructural properties have been a rich source of research for decades,⁹ but the question of the driving force of such a transition has not yet been fully resolved. In Nb, however, some of the typical precursors that usually occur at martensitic phase transitions were evidenced. This includes the occurrence of Kohn anomalies,¹⁰⁻¹⁴ anomalies in the elastic constants for different pressure ranges,¹² and Fermi surface nest-

ing, producing a Van Hove singularity in the electronic density of the states closed to the Fermi level.¹⁵ Potential metastable states that may be involved in martensitic phase transformations have been investigated for Nb in several theoretical studies, as this element is often used as prototype material to test simulation methods.^{11,16-18}

The best studied metastable phase of Nb is fcc.^{6,7,19} Other experimentally found metastable phases include hexagonal- ω (C32)⁴ and Pnma.⁵ The Pnma phase has been found in experiments.⁵ Moreover, the ω structure is observed in Nb under high pressure at temperatures around 77 K⁴ and in thin films.²⁰ These phases have been characterized by density functional theory (DFT)^{4,5} and, in addition, a metastable ω -like structure with vacancies.²⁰ Further studies in literature used DFT to calculate the energies of bcc, hcp and several topologically complex phases (TCP) such as A15, Laves phases and σ structures.¹⁸ In particular, the A15 phase in Nb-based intermetallic phases, such as Nb₃Sn, is famous for the occurrence of both martensitic phase transitions,²¹ the associated instabilities,²² and the occurrence of superconductivity. It is therefore worth examining this TCP phase in elemental Nb in more detail.

Diffusionless transition paths of martensitic transformations among these phases have been studied, particularly the transition from bcc to fcc (Bain path),²³⁻²⁵ and from bcc to hcp.²⁶ Complex indirect transition paths have been reported from hcp and bcc to intermetallic phases, such as Laves phases,^{27,28} and by means of kinetic Monte Carlo simulations from bcc to A15.²⁹ For Nb, however, other metastable phases are lower in energy and the possible transition paths are yet unknown.

A peculiarity of Nb experimental works is that Nb crystals are usually contaminated with Ta. The reason is

that Nb and Ta have common natural occurrences and that their separation is costly. Both elements are chemically similar, including their crystal structure.³⁰ Similar metastable phases occur in Nb and Ta, e.g., Pnma.³¹ Such additions of Ta have been found to lower the formation energy of metastable TCP phases of Nb¹⁸ while the influence on other known metastable phases of Nb is still unknown.

Within this work, we systematically revisit and compare the energies of metastable phases and the details of the diffusionless transition paths connecting these to bcc, both for Nb and the solid solution of Nb_(1-x)Ta_x. We find that Pnma, A15 and σ phase are lower in energy than the bct phase and also the energy barrier for the bcc to Pnma transition is 0.2 eV lower than the transition barrier from bct to fcc. Furthermore, the bcc to ω path shows an additional local energy minimum if extrapolated to larger values of strain. This configuration turns out to correspond to an easy deformation, but it is not stable against the relaxation to a bcc structure strained along [111].

II. METHOD

A. Technical details

Density-functional theory (DFT) simulations are performed with the abinit package.³² All calculations are done with primitive cells and Ta substitution is determined with the smallest possible cell up to a size of $2 \times 2 \times 2$. The results are determined with the generalized gradient approximation (GGA) using the Perdew-Burke-Ernzerhof (PBE) exchange-correlation functional³³ in connection with optimized norm-conserving Vanderbilt pseudopotential (ONCVSP) from PseudoDojo³⁴ with the valence electron configuration $4d^4 5s^1$ for Nb and $4f^{14} 5d^3 6s^2$ for Ta. The stopping criterion for the self-consistent calculations is a difference in total energy of $2.72 \cdot 10^{-7}$ eV. The volume and ionic positions of all structures are relaxed simultaneously with a tolerance on the maximal force of 2.5×10^{-3} eV/Å and a smearing parameter for the total energy of 95 eV, considering a temperature of smearing of 0.272 eV, which is equivalent to 3.15 K. The k -mesh is $14 \times 14 \times 14$ and a cutoff energy of 1088.45 eV results in an energy convergence of 0.172 eV.

Density-functional perturbation theory (DFPT) is used to determine phonon spectra and the phonon density of states. As an insufficient sampling of q -space for bcc Nb results in the extrapolation to imaginary phonon modes,³⁷ we chose a grid of $8 \times 8 \times 8$ which is sufficient to correctly reproduce the experimental and theoretical data from literature. Furthermore, we raise the threshold to a difference in potentials up to 10^{-18} , the k -mesh to $16 \times 16 \times 16$ and decreased the temperature of smearing to 0.136 eV (corresponds to 1.57 K). The k -mesh and q -grid for the other structures are scaled according to their

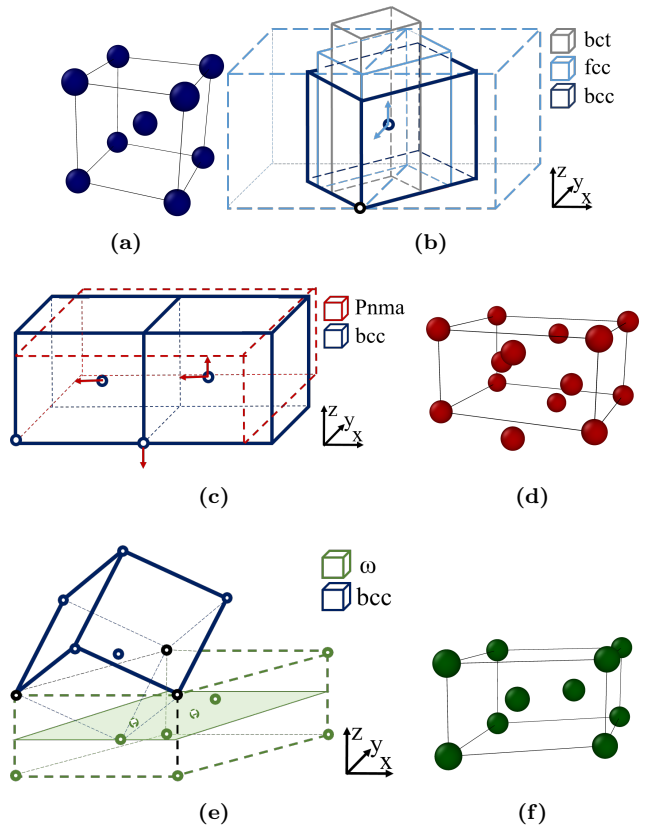


FIG. 1: Schematic representation of (a) the unit cell of the bcc ground state of Nb and the diffusionless transition paths to (b) fcc ($c/a = \sqrt{2}$, light blue) and bct (gray) as well as (c) Pnma (red) and (e) hexagonal ω (green) (d) and (f) show the unit cells of the relaxed Pnma and ω phases, respectively.

lattice vectors. The phonon contribution to Helmholtz free energy F_{phon} is calculated according to Lee et al.³⁸

$$F_{\text{phon}}(T) = 3nNk_B T \int_0^{\omega_L} \ln(2 \sinh \frac{\hbar\omega}{2k_B T}) g(\omega) d\omega \quad (1)$$

with the number of atoms per unit cell n , the number of unit cells N , the Boltzmann constant k_B and temperature T . ω_L is the largest frequency in the phonon spectra. Without anharmonic effects and thermal expansion, the total free energy $F_{\text{total}}(T)$ is approximately given as

$$F_{\text{total}}(T) = E_{\text{tot}}(T = 0 \text{ K}) + F_{\text{phon}}(T). \quad (2)$$

For comparison we compute selected properties also with the VASP package³⁹⁻⁴¹ using the high-throughput environment from Ref. 18. We use the PBE functional³³ as in the abinit calculations but the projector-augmented wave method⁴² and pseudo-potentials with s semicore states for Nb and p semicore states for Ta. With a planewave cut-off energy of 500 eV and a k -point density of 0.018 \AA^3 we achieve similar convergence of the total energy differences as in our calculations with abinit.

TABLE I: List of labels, space groups, lattice parameters a , tetragonal ratios c/a and energy differences to bcc of the (meta)-stable phases of interest. Available values from literature are added for comparison. Pnma_{max} and ω' refer to extrema from calculated transition paths (see Section III B). All values are based on PBE (\dagger : abinit, $*$: VASP), except Refs. 16 and 23 which are based on LDA. If not noted in brackets $a = b$. The tetragonal ratio of Pnma, ω and ω' in a pseudo-cubic unit cell are 1.73, 0.83 and 0.89, respectively.

Label	Space group	c/a (b/a)	a (\AA)	V ($\text{\AA}^3/\text{atom}$)	ΔE (meV/atom)	Ref.
bcc	$Im\bar{3}m$	1	3.30		0.0	²⁴
		1	3.31	18.11	0.0	this work*
		1	3.30	18.09	0.0	this work \dagger
σ	$P4_2/mnm$	0.53	10.18	18.57	82	this work*
		0.53	10.18	18.55	83	this work \dagger
A15	$Pm\bar{3}n$	1	5.29		104	¹⁷
		1	5.29	18.56	103	this work*
		1	5.29	18.60	105	this work \dagger
Pnma	$Pnma$	0.88 (0.52)	5.11		_35	5
		0.90 (0.52)	5.39	18.36	111	this work*
		0.89 (0.51)	5.41	18.32	119	this work \dagger
ω'	$P\bar{3}m1$	0.51	5.02	18.60	121 _36	this work \dagger
bct	$I4/mmm$	1.8	2.74		180	²³
		1.79	2.74	18.45	143	this work*
		1.77	2.71	18.48	143	this work \dagger
ω	$P6/mmm$	0.547	4.88		201	¹⁷
		0.548	4.88	18.45	199	this work*
		0.550	4.88	18.47	202	this work \dagger
A13	$P4_132$	1	-		286	¹⁶
		1	7.21	18.69	210	this work*
		1	7.14	18.77	223	this work \dagger
Pnma_{max}	$Pnma$	0.67 (0.50)	6.02	18.72	234	this work \dagger
hcp	$P6_3/mmc$	1.82	2.86		297	¹⁷
		1.83	2.85	18.64	294	this work*
		1.82	2.87	18.66	294	this work \dagger
fcc	$Fm\bar{3}m$	1	4.21		324	¹⁷
		1	4.21	18.74	323	this work*
		1	4.21	18.77	323	this work \dagger

Besides bcc, bct, ω , Pnma, A13, A15, and σ phases shown in Fig. 2, we also consider the Laves phases C14, C15, C36 and the structures μ and χ . Ordered binary structures based on fcc or hcp are excluded due to the expected comparably high formation energy.¹⁸ For the considered phases, all occupations of Nb and Ta on the Wyckoff sites are included in the DFT calculations, e.g., $2^5 = 32$ DFT calculations for the σ phase with five Wyckoff sites. We assess the relative stability of the different structures and stoichiometries based on the heat of formation

$$\Delta H_f = \frac{E_{\text{tot}} - N_{\text{Nb}}E_{\text{Nb}} - N_{\text{Ta}}E_{\text{Ta}}}{N}, \quad (3)$$

with N_{Nb} (N_{Ta}) and E_{Nb} (E_{Ta}) the number of Nb (Ta) atoms and their energies in the bcc phases. For pure systems this equation reduces to the energy difference of a structure to the bcc ground state, i.e., ΔE in Tab. I.

B. Transformation paths

We study potential martensitic transition paths from bcc to fcc, ω and Pnma using a linear interpolation of the lattice constants a_i to the final state as

$$a_i(\Delta) = (1 - \Delta) \cdot a_i^{\text{initial}} + \Delta \cdot a_i^{\text{final}} \quad (4)$$

with varying Δ from 0 to 1, see Fig. 1. The bcc to fcc transition is fully characterized by the lattice constants (see Fig. 1 (a)). For the bcc to Pnma and ω transition path, we additionally interpolate the internal atomic degrees of freedom linearly. The interpolation along the bcc- ω path (Fig. 1 (c)), corresponds to an anti-parallel shift of two of three atoms along z-direction from $\Delta_z = 0$ for bcc to $\Delta_z = \pm 1/6$ for ω phase. Only in the ω phase, both these atoms are in the same z-plane of the hexagonal lattice (i.e. the same [111] plane of bcc) and the

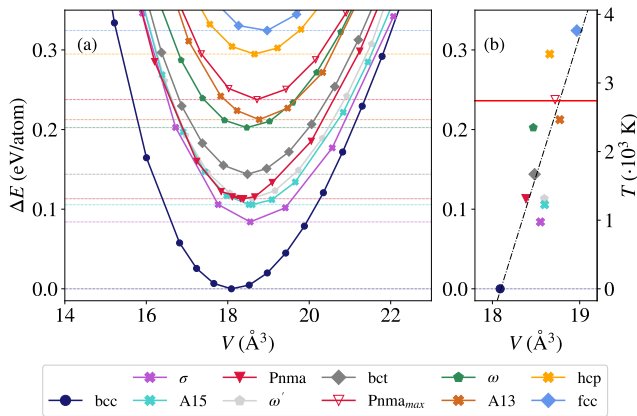


FIG. 2: (a) Energy-volume curves of the (meta-)stable phases of Nb of interest. The energy per atom is given relative to the bcc ground state and (b) a reduced graphical representation with the minima for the selected structures only. The thick red horizontal line in (b) marks the melting temperature ($T_m = 2741$ K) of Nb,⁴⁵ according to the second axis with an estimation for T using $E = k_B T$. The black line represents a linear fit of the data.

symmetry is P6/mmm while the symmetry is reduced to $P\bar{3}m1$ on the path.^{43,44}

Note, that the transition from bcc to Pnma contains two unit cells of bcc, and a_{bcc} consequently must be doubled, see Fig. 1 (b). Two atoms shift by Δ_x and one atom each shift by Δ_x and Δ_{z1} and another by Δ_{z2} . For the relaxed Pnma structure we find values of $\Delta_x = 0.01$, $\Delta_{z1} = -0.2$, $\Delta_{z2} = 0.04$, respectively. The atomic environment of the Pnma phase is thereby similar to that of the bcc state, but the 8-fold coordination (with a distance of 2.86 Å) splits into four nearest neighbours with average distances about 2.80 Å and four nearest neighbours with average distance of 2.97 Å. Further we extrapolate the range of Δ to smaller or larger values to explore the energy landscape around the given states and analyse the A15 phase under tetragonal distortion in the range of $0.8 < c/a < 1.2$.

III. RESULTS

A. Comparison of meta-stable phases

We consider all Nb structures listed in Tab. I. Figure 2 (a) shows their energy differences to the ground state, ΔE , as a function of volume V per atom. In agreement to literature we find bcc as the ground state structure while fcc is the least favourable of all tested configurations and about 330 meV higher in energy. Still this phase has been observed in experiments underlining the importance of meta-stable Nb phases with lower energies. Although the energy of the fcc phase is reduced by tetragonal distortion to the bct phase, A15 and Pnma structures are even more favourable with energy differ-

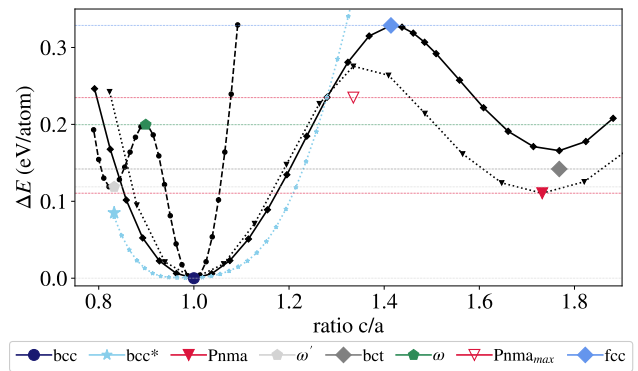


FIG. 3: Energy landscape for the deformation of the bcc cubic structure with $c/a = 1$ along (a) the Bain path to fcc (solid line with diamonds), (b) the path to Pnma (dotted line with triangles) and (c) the path to ω (dashed line with circles). The lattice parameters of Pnma and ω are given in a pseudo-cubic unit cell. All colored symbols indicate structures whose volumes and positions of atoms are relaxed, unlike the other data points. For bcc in the hexagonal ω phase (bcc*), furthermore the energy landscape for tetragonal distortion is shown in light blue.

ences of about 105 meV and 119 meV relative to bcc only, respectively. The ω , A13, and hcp phases are energetically between bct and fcc.

Our calculations show that the σ phase is even more favourable being only slightly less than 80 meV above the ground state. As we discuss in Sec. III B, the bcc to ω -phase shows an additional local minimum, which we have added as ω' for completeness. This configuration shows a minimum of the energy vs. volume curve only 121 meV higher in energy than bcc. As discussed below the structure is however not stable against atomic relaxation.

The same data is reduced to the minima of the $E(V)$ curves in Fig. 2 (b). The energy of the metastable phases scales approximately linearly with the volume. Although, Pnma and ω have been predicted as high-pressure phases their ground state volumes without pressure is larger than the ground state volume of bcc. The bcc structure is not only the energetic ground state for its equilibrium volume but also in the studied volume range of 15 to 22 Å³. Under lattice expansion between 21 Å³ and 22 Å³ the energy differences between bcc and σ and A15 are however systematically reduced. Furthermore, in this volume range ω and A13 phases as well as Pnma and bct phases are close in energy. On the other hand, none of the phases comes close to bcc for reduced volumes while the energy differences between ω' , Pnma, A15 and σ phases are reduced.

B. Transformation paths

To depict possible diffusionless phase transitions of Nb, we study the energy landscape for a continuous defor-

mation from bcc to meta-stable structures. The energy maxima on these paths give an upper bound for the energy barriers of the transitions. Note, that the real energy barriers can be smaller due to their dependence on temperature or more complex transition paths. As reference we start with the classical Bain path from bcc to fcc (solid lines in Fig. 3). In agreement with literature we find that fcc is a local maximum on the transformation path and the second minimum, the bct structure with $c/a = 1.768$ is 143 meV higher in energy than bcc, see Tab. I.

In the following we restrict ourselves to the low energy structures shown in Fig 1: (a) bcc, (d) Pnma and (f) ω . The dotted lines in Fig. 3 show the bcc to Pnma path. On this path, only the two energy minima related to bcc and Pnma occur and both states are separated by an energy barrier of 234 meV which is about 89 meV lower than the fcc state. Surprisingly, the ω phase is not even a local minimum of energy on the bcc to ω path but rather a local energy maximum. By extrapolation of Δ we find an energy minimum (ω') with $\Delta z = 0.28$ and $c/a = 0.832$ only 121 meV higher in energy than the bcc ground state. Note that this anomaly has not been found for a variation of Δz with fixed tetragonal ratio⁴⁴ and the structure differs from the modulated ω structure with vacancies discussed in the supplementary material from Ref. 20. Although this monoclinic configuration also shows the typical energy volume curve of a meta-stable state, see Fig. 2, the atomic positions are not protected against atomic relaxation by symmetry. Only the ω phase with P6/mmm symmetry is a meta-stable state, while the atomic positions relax to the bcc-like structure with $z = 0$ for all other initial values of z .

The distorted bcc state at $c/a = 0.832$, which we call bcc* in the following, is only 85 meV higher in energy than bcc and may thus be a favorable distortion of the bcc phase. For this reason we sample the energy for the tetragonal distortion of the bcc* to the bcc state as shown in Fig. 2. Our calculations show that the energy penalty for the distortion along the [111] direction is considerably smaller than for the bcc to fcc path.

Given the lack of information on transition paths among the metastable states, we additionally verified if tetragonally distorted structures are possible for other metastable phases of Nb. Particularly the cubic A15 phase is low in energy and we also study its tetragonal distortion, see Fig. 2. But even with a fine resolution of $\Delta c/a = 2 \cdot 10^{-4}$ we could not observe any additional local minima or higher-order extrema under tetragonal distortion. The increase of energy with tetragonal distortion is similar to the classical Bain path.

C. Phonon spectra

For a comprehensive picture of the low-energy phases, we analyze the phonon spectra of bcc, bcc* (bcc phase distorted along [111] with $c/a = 0.832$), ω' and Pnma.

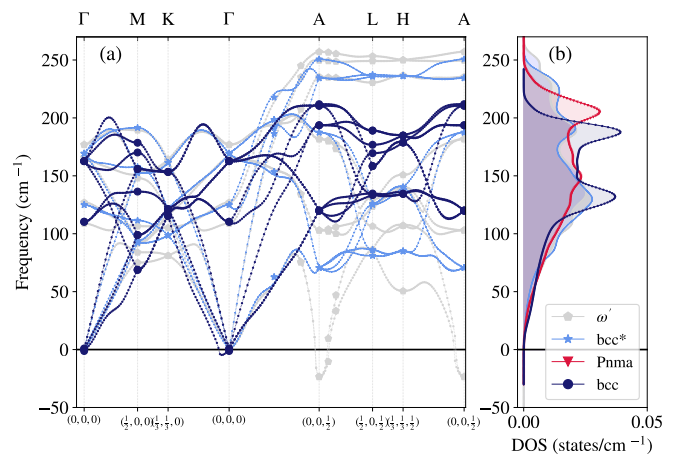


FIG. 4: (a) Phonon spectra of the ω' phase (grey) bcc* (light blue) and bcc (dark blue). The dots mark q-points used in the DFPT framework and lines are interpolations. (b) Comparison of the phonon densities of state (DOS) per atom for ω' , bcc*, Pnma (red) and bcc.

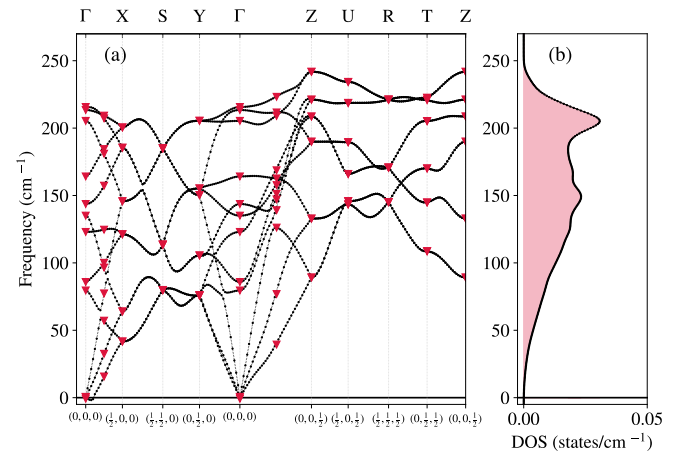


FIG. 5: (a) Phonon spectrum of the Pnma phase. The dots mark q-points used in the DFPT framework and lines are interpolations. (b) The phonon densities of state (DOS) per atom.

While the phonon spectra of the bcc and Pnma structures calculated by us correspond to those published in literature,^{5,46} we are not aware of calculated phonon spectra of (distorted) ω phases which are summarized in Fig. 4 (a). As reference we also added the phonon spectra of bcc in the same representation.

Indeed, the ground state, bcc, only shows stable phonon modes. However, there are indications, that the structure is close to an instability. Particularly, we can reproduce the Kohn anomaly at $(0.142, -0.142, 0.142)$ predicted by Landa et al.¹² Note, that in the representation in Fig. 4 (a) this point is located on the $\Gamma \rightarrow M$ path. Furthermore we can reproduce the decrease of the transversal acoustic branch in the phonon spectra at

(1/3, 0, 1/3) in the [111] direction associated with the bcc to ω transition.^{44,47}

The metastable Pnma phase also shows no soft phonons, see Fig. 5 (a). Compared to bcc the change in slope on the $\Gamma \rightarrow Z$ path is reduced. Furthermore, due to the lower symmetry of Pnma one has to distinguish X, Y and Z direction and for the former two we see no change in slope on the corresponding paths with the given resolution. Analogous to bcc and Pnma, also bcc* does not show soft phonon modes. Under the hexagonal distortion the change of the slope on the $\Gamma \rightarrow M$ path vanishes, both for bcc* and ω' , while the lowest $\Gamma \rightarrow A$ branch shows a similar feature. Moreover, for all high-symmetry points except M, the transversal branches are lowered in energy if going from bcc to ω' and bcc*. As discussed in Sec. IIB the ω' structure, although being a local energy minimum on the bcc- ω path is not a stable structure and thus the phonon spectrum shows negative frequencies at A (0,0,1/2).

Figure 4 (b) compares the resulting phonon density of states of all four structures normalized with the number of atoms in the system. Over a large frequency range from 125 cm^{-1} to 200 cm^{-1} , the bcc phase shows the largest density of states with two pronounced peaks around 135 cm^{-1} and 190 cm^{-1} . With decreasing symmetry going from bcc to bcc* and ω' the degeneracies of the modes in [100] direction are lifted and the peaks in the DOS are broadened. The distortion of the structure to ω' furthermore results in two additional peaks at 80 cm^{-1} and 230 cm^{-1} and a low-frequency tail. Below frequencies of 125 cm^{-1} , the ω' phase thus exhibits the highest density of states. A lifting of degeneracies in the modes in [100] direction can also be seen for the Pnma phase. Also here, we find higher frequencies in the spectrum and less pronounced peaks in the DOS. For the Pnma phase the largest DOS is found at about 210 cm^{-1} and the increase of the weight of the low-frequency tail of the DOS is slightly larger than for ω' .

However, none of the phases has a substantially larger phonon DOS in a suitable frequency range and the low-frequency tails of the DOS are not sufficient to reduce the free energy and to stabilize one of the phases relative to bcc at finite temperatures. Note that we calculated the free energies within the harmonic approximation and thus higher order effects are not accounted in this estimate.

D. Ta-substitution

In order to enable a close comparison of our results with experimental works, we additionally consider the influence of Ta on the metastable phases of Nb, the most common impurity in Nb samples for experiments.

Figure 6 compares the energy landscapes of pure Nb (black) and Ta (light green) along the classical Bain path (a) and the paths connecting bcc (b) and Pnma (c) and ω phases. In all cases, the energetic ground state is the

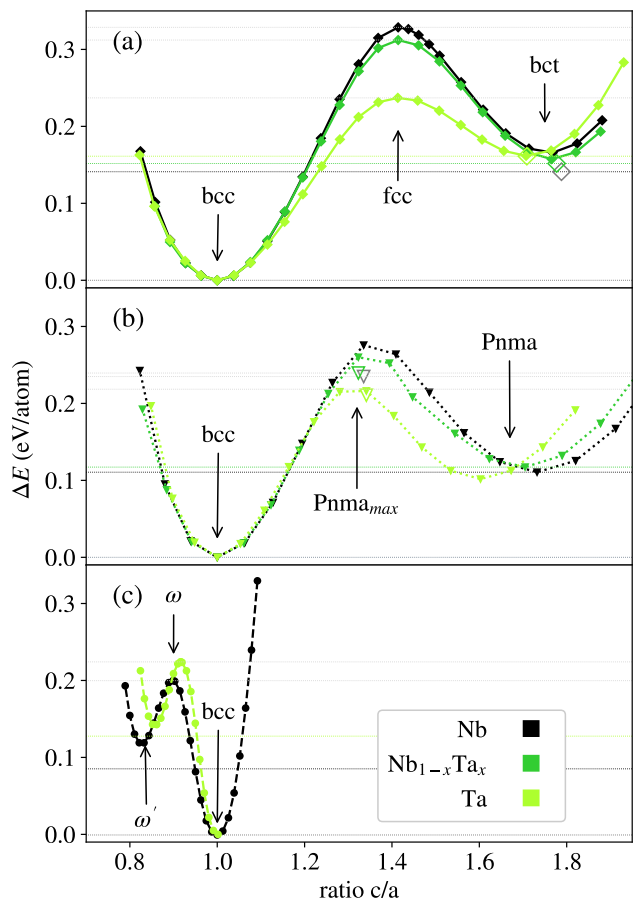


FIG. 6: Impact of Ta-substitution with a concentration of $x = 0.25$ on (a) the bcc-bct Bain transition path, (b) the bcc to Pnma transition path with two bcc unit cells and a random Ta substitution and (c) the bcc to ω transition path. Note that volume and atomic positions have been fixed on the transition path (filled symbols) and open symbols indicate the energy of the energy maximum after corresponding relaxation.

bcc state with $c/a = 1$ and the other local energy minima are not considerably lowered by Ta. The ratio of the lattice constants c/a is smaller for Ta compared to Nb (-0.07 for bct, and -0.13 for Pnma), but slightly increased for ω' by 0.02 . For bct (panel a) and Pnma (panel b), the energy barrier for the transformation is 91 meV and 24 meV smaller for Ta compared to Nb. However, the changes of the energy landscapes under partial substitution are small. Exemplary results for 25% Ta are added in panels (a) and (b) in dark green. Even for this large concentration, the energy differences between the pure and substituted materials are below 16 meV and 4 meV at the transition barrier. For the bcc to ω transition, the barrier is not smaller for Ta compared to Nb and for both elements the structure at the second minimum is not stable against atomic relaxation.

The influence of Ta on the structural stability of all phases of interest across the complete range of chemical

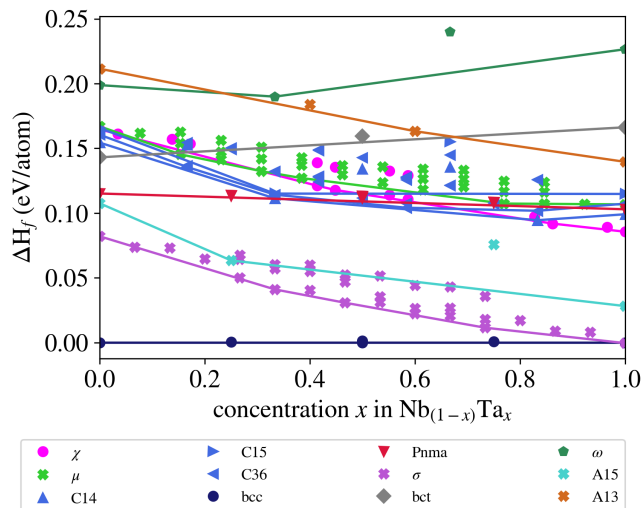


FIG. 7: Structural stability of Nb-Ta phases obtained by DFT with permutation of Nb and Ta atoms on Wyckoff sites of bcc, bct, C32, A13 and the topological complex phases (TCP) phases A15, C14, C15, C36, μ , χ and σ . The lines represent the convex hulls of the individual phases to guide the eye.

compositions is shown in Fig. 7 in terms of the formation energies ΔH_f . The relative stability for pure Nb is identical to the sequence of minima observed in the energy-volume curves in Fig. 2. The variation across the Nb-Ta chemical range is consistent with previous DFT calculations¹⁸ using an LDA exchange-correlation functional although PBE shows slightly lower formation energies ΔH_f . Comparing pure Ta to Nb, the phase sequence bcc, σ , A15, Pnma, bct and ω is still present. However, the A13, σ and A15 phases are considerably lowered in energy. The σ phase is very close to bcc, in line with the experimental characterization of β -Ta as σ phase.⁴⁸ The formation energies of the Pnma phase depend only weakly on the Ta concentration. For completeness also the formation energies of the Laves (C14, C15, C36), χ and μ phases are shown in Fig. 7. For Nb all these phases are higher in energy than bct. There is no sizeable stabilisation of the Laves and μ phases by Ta, while the χ phase becomes more favourable than the Pnma phase. The throughout positive values of ΔH_f indicate that there is no stable ordered structure, in line

with the bcc solid-solution region in the phase diagram.

Thus Ta indeed reduces the energy barrier for the bcc to bct or Pnma transitions but quantitatively the effect is small. We would furthermore expect that alloying Nb with small amounts of Ta may foster the formation of A13 or σ phases while an enhanced formation of Pnma is unlikely.

IV. SUMMARY AND CONCLUSIONS

The question of potential metastable phases in Nb was raised anew by high-resolution experimental data suggesting a martensitic phase transition.⁸ To better understand the energy landscape of Nb, we determined the ground states for chosen metastable phases using DFT and analysed possible transition paths connecting these with the bcc ground state. We find that the metastable σ and A15 phases are lowest in energy followed by Pnma, bct and A13. Both the bcc to Pnma and bcc to ω path are more favourable than the more commonly discussed Bain path to fcc. Additionally, straining bcc along the hexagonal [111] direction, we find a potential deformed state ω' being low in energy.

Since Ta impurities are common in Nb, we also investigated the role of Ta on the energy landscape of the metastable phases. The energy barriers for the bcc to bct and Pnma transition are reduced. In pure Ta, the σ phase is practically as low in energy as the bcc phase. Thus, for high Ta concentrations, this is important and should be further investigated in the future.

Otherwise, considering our DFT study, we suggest that effects that could come from the microstructure not detected here - like stabilization of a metastable phase by twinning - may trigger phase transitions or modify the atomic structure in large parts of an experimental sample, explaining the experimentally found martensitic phase transition.

ACKNOWLEDGMENTS

We thank Anna Böhmer and Ralf Drautz for fruitful discussion.

¹ J. A. Sauls, M. Zarea, and H. Ueki. Effects of Anisotropy and Disorder on the Superconducting Properties of Niobium. *Frontiers in Physics*, 11:1269872, 2023.
² G.J. Sellers, A.C. Anderson, and H.K. Birnbaum. The anomalous heat capacity of superconducting niobium. *Physics Letters A*, 44(3):173, 1973.
³ V. Struzhkin, Y. Timofeev, R. Hemley, and H. Mao. Superconducting T_c and Electron-Phonon Coupling in Nb to 132 GPa: Magnetic Susceptibility at Megabar Pressures.

Physical Review Letters, 79(21):4262, 1997.

⁴ X. Li, Q. Zhao, Q. Wang, Y. Tian, H. Zhou, and J. Wang. Shear band mediated ω phase transformation in Nb single crystals deformed at 77 K. *Materials Research Letters*, 9(12):523, 2021.

⁵ D. Errandonea, L. Burakovsky, D. L. Preston, S. G. MacLeod, D. Santamaría-Perez, S. Chen, H. Cynn, S. I. Simak, M. I. McMahon, J. E. Proctor, and M. Mezouar. Experimental and theoretical confirmation of an or-

- thorhombic phase transition in niobium at high pressure and temperature. *Communications Materials*, 1(1):60, 2020.
- 6 Q. Wang, J. Wang, J. Li, Z. Zhang, and S. X. Mao. Consecutive crystallographic reorientations and superplasticity in body-centered cubic niobium nanowires. *Science Advances*, 4(7):eaas8850, 2018.
 - 7 P. P. Chattopadhyay, P. M. G. Nambissan, S. K. Pabi, and I. Manna. Polymorphic bcc to fcc transformation of nanocrystalline niobium studied by positron annihilation. *Physical Review B*, 63(5):054107, 2001.
 - 8 R. K. Bollinger, B. D. White, J. J. Neumeier, H. R. Z. Sandim, Y. Suzuki, C. A. M. dos Santos, R. Avci, A. Migliori, and J. B. Betts. Observation of a Martensitic Structural Distortion in V, Nb, and Ta. *Physical Review Letters*, 107(7):075503, 2011.
 - 9 A. Grünebohm, A. Hütten, A. E. Böhmer, J. Frenzel, I. Eremin, R. Drautz, I. Ennen, L. Caron, T. Kuschel, F. Lechermann, D. Anselmetti, T. Dahm, F. Weber, K. Rossnagel, and G. Schierning. A Unifying Perspective of Common Motifs That Occur across Disparate Classes of Materials Harboring Displacive Phase Transitions. *Advanced Energy Materials*, 13(30):2300754, 2023.
 - 10 Y. Nakagawa and A. D. B. Woods. Lattice Dynamics of Niobium. *Physical Review Letters*, 11(6):271, 1963.
 - 11 S. de Gironcoli. Lattice dynamics of metals from density-functional perturbation theory. *Physical Review B*, 51(10):6773, 1995.
 - 12 A. Landa, P. Söderlind, I. Naumov, J. Klepeis, and L. Vitos. Kohn Anomaly and Phase Stability in Group VB Transition Metals. *Computation*, 6(2):29, 2018.
 - 13 F. Tidholm, O. Hellman, N. Shulumba, S. I. Simak, J. Tasnádi, and I. A. Abrikosov. Temperature dependence of the Kohn anomaly in bcc Nb from first-principles self-consistent phonon calculations. *Physical Review B*, 101(11):115119, 2020.
 - 14 P. Aynajian, T. Keller, L. Boeri, S. M. Shapiro, K. Habicht, and B. Keimer. Energy gaps and Kohn anomalies in elemental superconductors. *Science*, 319(5869):1509, 2008.
 - 15 Zenghui Liu and Jiaxiang Shang. First principles calculations of electronic properties and mechanical properties of bcc molybdenum and niobium. *Rare Metals*, 30:354, 2011.
 - 16 M. J. Mehl and D. A. Papaconstantopoulos. Applications of a tight-binding total-energy method for transition and noble metals: Elastic constants, vacancies, and surfaces of monatomic metals. *Physical Review B*, 54(7):4519, 1996.
 - 17 M. R. Feller, H. Park, and J. W. Wilkins. Force-matched embedded-atom method potential for niobium. *Physical Review B*, 81(14):144119, 2010.
 - 18 T. Hammerschmidt, A. F. Bialon, D. G. Pettifor, and R. Drautz. Topologically close-packed phases in binary transition-metal compounds: matching high-throughput *ab initio* calculations to an empirical structure map. *New Journal of Physics*, 15(11):115016, 2013.
 - 19 M. Sasaki, M. Koyano, H. Negishi, and M. Inoue. F.c.c. niobium films grown by halide chemical vapour deposition on ultrasound-vibrating substrates. *Thin Solid Films*, 158(1):123, 1988.
 - 20 J. Lee, Z. Sung, A. A. Murthy, A. Grassellino, A. Romanenko, N. S. Sitarman, and T. A. Arias. Stress-induced structural changes in superconducting Nb thin films. *Physical Review Materials*, 7:L063201, 2023.
 - 21 A. Godeke. A review of the properties of Nb₃Sn and their variation with A15 composition, morphology and strain state. *Superconductor Science & Technology*, 19, 2006.
 - 22 B. Sadigh and V. Ozoliņš. Structural instability and electronic excitations in Nb₃Sn. *Physical Review B*, 57(5):2793, 1998.
 - 23 S. Schoenecker. *Theoretical studies of epitaxial Bain paths of metals*. dissertation, Technische Universität Dresden, 2011.
 - 24 N. O. Nnolim, T. A. Tyson, and L. Axe. A theoretical study of the structural phases of Group 5B – 6B metals and their transport properties. *Journal of Applied Physics*, 93:4543, 2003.
 - 25 P. J. Craievich, M. Weinert, J. M. Sanchez, and R. E. Watson. Local stability of nonequilibrium phases. *Physical Review Letters*, 72(19):3076, 1994.
 - 26 P. J. Craievich, J. M. Sanchez, R. E. Watson, and M. Weinert. Structural instabilities of excited phases. *Physical Review B*, 55(2):787, 1997.
 - 27 A. R. Natarajan and A. Van der Ven. Connecting the Simpler Structures to Topologically Close-Packed Phases. *Physical Review Letters*, 121(25):255701, 2018.
 - 28 S. K. Kolli, A. R. Natarajan, and A. Van der Ven. Six new transformation pathways connecting simple crystal structures and common intermetallic crystal structures. *Acta Materialia*, 221:117429, 2021.
 - 29 P. Xiao, D. Sheppard, J. Rogal, and G. Henkelman. Solid-state dimer method for calculating solid-solid phase transitions. *The Journal of Chemical Physics*, 140(17):174104, 2014.
 - 30 M. Nete, W. Purcell, and J.T. Nel. Separation and isolation of tantalum and niobium from tantalite using solvent extraction and ion exchange. *Hydrometallurgy*, 149:31, 2014.
 - 31 Y. Yao and D. D. Klug. Stable structures of tantalum at high temperature and high pressure. *Physical Review B*, 88(5):054102, 2013.
 - 32 X. Gonze, F. Jollet, F. Abreu Araujo, D. Adams, B. Amadon, T. Applencourt, C. Audouze, J.-M. Beuken, J. Bieder, A. Bokhanchuk, E. Bousquet, F. Bruneval, D. Caliste, M. Côté, F. Dahm, F. Da Pieve, M. Delaveau, M. Di Gennaro, B. Dorado, C. Espejo, G. Geneste, L. Genovese, A. Gerossier, M. Giantomassi, Y. Gillet, D.R. Hamann, L. He, G. Jomard, J. Laflamme Janssen, S. Le Roux, A. Levitt, A. Lherbier, F. Liu, I. Lukačević, A. Martin, C. Martins, M.J.T. Oliveira, S. Poncé, Y. Pouillon, T. Rangel, G.-M. Rignanese, A.H. Romero, B. Rousseau, O. Rubel, A.A. Shukri, M. Stankovski, M. Torrent, M.J. Van Setten, B. Van Troeye, M.J. Verstraete, D. Waroquiers, J. Wiktorski, B. Xu, A. Zhou, and J.W. Zwanziger. Recent developments in the ABINIT software package. *Computer Physics Communications*, 205:106, 2016.
 - 33 J. P. Perdew, K. Burke, and M. Ernzerhof. Generalized Gradient Approximation Made Simple. *Physical Review Letters*, 77:3865, 1996.
 - 34 D. R. Hamann. Optimized norm-conserving Vanderbilt pseudopotentials. *Physical Review B*, 88(8):085117, 2013.
 - 35 Note that only a rough estimate of the energy has been reported (200 meV/atom) in Ref. 5.
 - 36 Note that this phase is a minimum on the transition path, but not (meta)-stable.
 - 37 P. Souvatzis and O. Eriksson. *Ab initio* calculations of the phonon spectra and the thermal expansion coefficients of the 4d metals. *Physical Review B*, 77:024110, 2008.
 - 38 C. Lee and X. Gonze. *Ab initio* calculation of the ther-

- modynamic properties and atomic temperature factors of SiO₂ α -quartz and stishovite. *Physical Review B*, 51(13):8610, 1995.
- ³⁹ G. Kresse and J. Furthmüller. Efficiency of ab-initio total energy calculations for metals and semiconductors using a plane-wave basis set. *Computational Materials Science*, 6(1):15, 1996.
- ⁴⁰ G. Kresse and J. Furthmüller. Efficient iterative schemes for ab initio total-energy calculations using a plane-wave basis set. *Physical Review B*, 54:11169, 1996.
- ⁴¹ G. Kresse and D. Joubert. From ultrasoft pseudopotentials to the projector augmented-wave method. *Physical Review B*, 59:1758, 1999.
- ⁴² P. E. Blöchl. Projector augmented-wave method. *Physical Review B*, 50:17953, 1994.
- ⁴³ G. Aurelio and A. Fernández Guillermet. Interatomic distances in the stable and metastable bcc and omega structures of the transition metals: analysis of experimental and theoretical trends and correlations with Pauling's bond lengths. *Journal of Alloys and Compounds*, 292(1):31, 1999.
- ⁴⁴ J.E. Garcés, G.B. Grad, A. Fernández Guillermet, and S.J. Sferco. Theoretical study of the structural properties and thermodynamic stability of the omega phase in the 4d-transition series. *Journal of Alloys and Compounds*, 289(1):1, 1999.
- ⁴⁵ François Cardarelli. *Materials handbook: a concise desktop reference*. Springer London, 2008.
- ⁴⁶ G. D. Marzi. Electronic Band Structure, Lattice Dynamics, and Related Superconducting Properties of Niobium from First-Principles Calculations. Technical report, ENEA, 2016.
- ⁴⁷ H.E. Cook. A theory of the omega transformation. *Acta Metallurgica*, 22(2):239, 1974.
- ⁴⁸ A. Jiang, A. Yohannan, N.O. Nnolim, T.A. Tyson, L. Axe, S.L. Lee, and P. Cotec. Investigation of the structure of β -tantalum. *Thin Solid Films*, 437:116, 2003.